



Analysis of radioisotopic metal impurities generated in $[^{18}\text{O}]\text{H}_2\text{O}$ during ^{18}F production with cyclotron



D. Alloni^{1,2*}, M. Prata^{1,2}, B. Smilgys^{3,#}

¹LENA, Laboratorio Energia Nucleare Applicata, Università degli Studi di Pavia, Via Aselli 4, Pavia.

²INFN, Istituto Nazionale di Fisica Nucleare, Sezione di Pavia, Via Bassi 6, Pavia.

³INSTM, Consorzio Interuniversitario Nazionale per la Scienza e Tecnologia dei Materiali, Unità di Pavia, Via Taramelli 12, Pavia.

*Corresponding author: daniele.alloni@unipv.it
Presenting author: barbara.smilgys@unipv.it

Laboratorio Energia Nucleare Applicata
Università degli Studi di Pavia



Abstract - In this work we present a characterization of the radionuclidic impurities originated by proton irradiation of enriched water $[^{18}\text{O}]\text{H}_2\text{O}$ in a medical cyclotron through Monte Carlo simulations and experimental measurements. A set of standard samples of enriched water loaded in the cyclotron target cell have been irradiated at 30 μA proton current for one hour each and, after an appropriate cooling time, measured by HPGe gamma spectrometry. In this way it was possible to study the direct release of radionuclidic impurities from target components as well as the release as a function of target ageing. Previously to experimental measurements, Monte Carlo calculations with the Phits Code have been carried out to estimate the radionuclides generated within the target components (in particular Havar[®] foil) with the aim to identify the nuclides expected to be found in the irradiated water due to cell-to-water transmission mechanisms. Comparison between simulations data and experimental measurements by gamma spectrometry revealed that only a very small amount of the radionuclides produced in the target window are released in the enriched water through corrosion/erosion effects, while the release decreases with increasing aging of the target.

Introduction

- Cyclotron-based radionuclide production and chemical synthesis of the marked molecule constitute the two main processes of the production of the most common radionuclides for Positron Emission Tomography (PET) (Alauddin, 2012) such as $[^{18}\text{F}]\text{2-fluoro-2-deoxy-D-glucose}$ $[^{18}\text{F}]\text{FDG}$. In the production process, (p,n) nuclear reactions induced by 18 MeV proton beam into a target which contains the $[^{18}\text{O}]$ -enriched water sample give rise to the production of ^{18}F (IAEA, 2009).
- Interactions of protons with the materials of the target cell and material activation due to the neutron secondary radiation field produced by the (p,n) reaction (IAEA, 2011), causes the formation and **release of radionuclide pollutants** during the irradiation process (Bowden et al., 2009; Gillies et al., 2006).
- The estimation and quantification of these pollutants is an important issue from a radiological point of view because these determine the most efficient way to remove them during $[^{18}\text{F}]\text{FDG}$ synthesis procedures for the final radiopharmaceutical product to be administered to patients, and, furthermore, to maximize yields during ^{18}F fluorination reactions (Tewson et al., 1988).

Fluorine-18 production with cyclotron

- The **cyclotron** installed at the **Applied Nuclear Energy Laboratory (LENA)** of the University of Pavia, is an IBA cyclotron (model Cyclone[®] 18/9) set up for 18 MeV proton bombardment of a highly ^{18}O -enriched H_2O target ($^{18}\text{O}>98.0$ Atom %, provided by Huayi Isotopes Co.) with a nominal 30 μA beam current.

Formation of radionuclides inside the target cell

- During proton bombardment the **target cell** (Figure 1) is the part that is most exposed to the direct proton beam which, with an initial energy of 18 MeV, stops entirely in the loaded enriched water volume, after traversing the target collimator and the two windows (Figures 2 and 3). The consequent release of heat in enriched water (about 160 W/cm^2 , reaching a temperature of about 240°C at 20 bar standard irradiation pressure) causes **erosive action processes** which lead to damage to the niobium cell internal surface, while the windows, in particular the Havar[®] one, which is in contact with enriched water, is submitted to **direct proton beam interaction as well as erosive water action**.

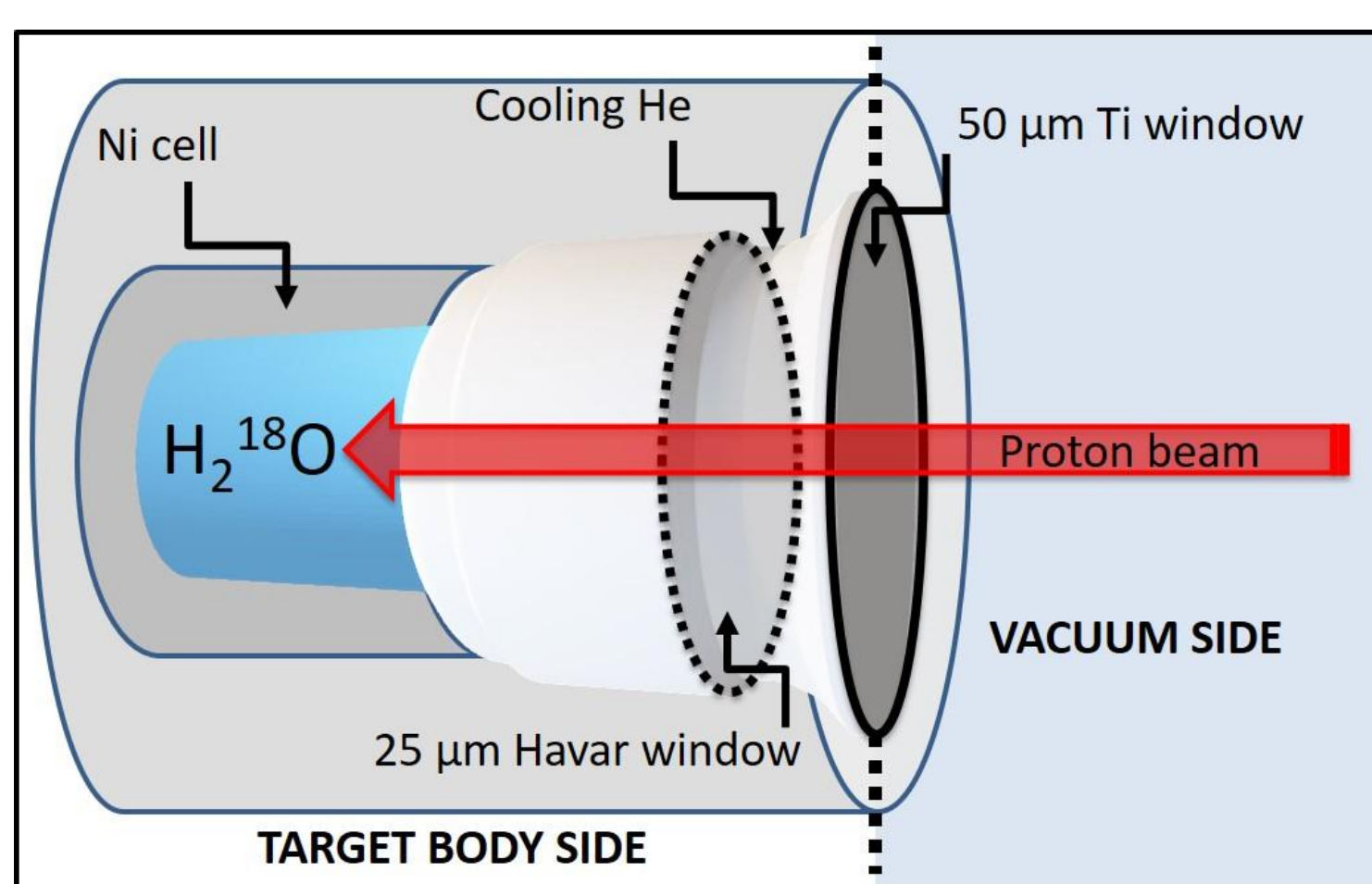


FIGURE 1: structure of the target cell



FIGURE 2: target assembly

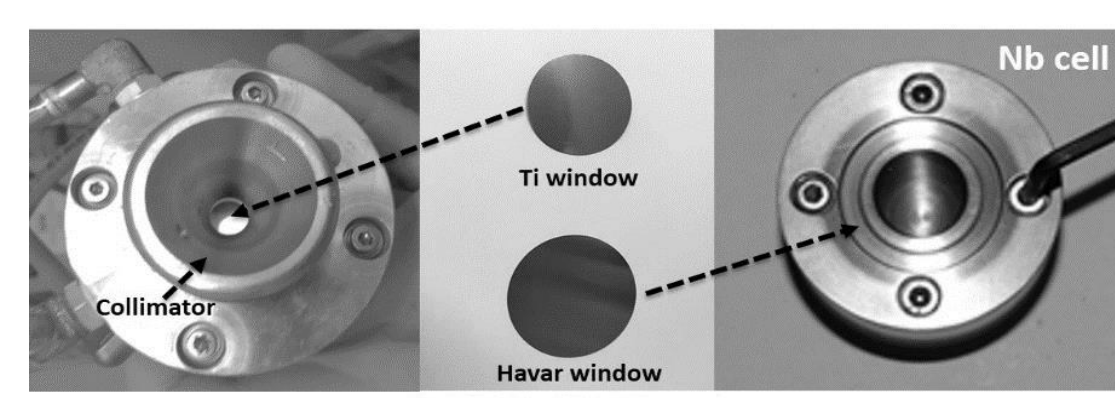


FIGURE 3. Left: Target collimator. Centre: Target windows. Right: Target cell

- Protons and neutrons activation processes cause the formation of radionuclides in cell target and Havar[®] windows which in turn **contaminate the enriched water volume**. In general, the release amount of these pollutants is related to the damage level of the Havar[®] window.
- The presence of these radiochemical pollutants affects the final yield since they are competitors and/or inhibitors in all its stages of the subsequent FDG synthesis process.
- In this work we focus on the **Monte Carlo and experimental characterization of the radionuclidic impurities contained in the proton- irradiated $[^{18}\text{O}]\text{H}_2\text{O}$ originated in the Havar[®] window**. Monte Carlo simulations, as a support to our experimental measurements, allowed an estimation of a list of the main radionuclides produced in the target Havar[®] window to be compared with experimental measurements.

Target modelling and Monte Carlo simulations

- Monte Carlo calculation** have been performed with the **PHITS** code (Particle and Heavy Ion Transport code System (Sato et al., 2013) coupled with the subroutine estimator D-Chain to simultaneously calculate the activity of radionuclides inside the Havar[®] window exposed to the proton beam as well as its time evolution during bombardment and after the end of beam
- The **target cell model** (see Figure 4) is composed by niobium body and Havar[®] window (thickness 25 μm , density 8.3 g/cm^3 ; typical composition (Goodfellow[®] disks): 42.5% Co, 20% Cr, 13% Ni, 2.8% Tg, 2.4% Mo, 1.6% Mg, 0.2 % C, plus residual Fe).

- Monte Carlo calculations of the specific activities for the dominant radionuclides (Table 1) and their time evolution (Figure 5) generated in the Havar window have a **statistical uncertainty less than 5 %**. A Very detailed geometrical and material structure of the target has been used (Figure 4).

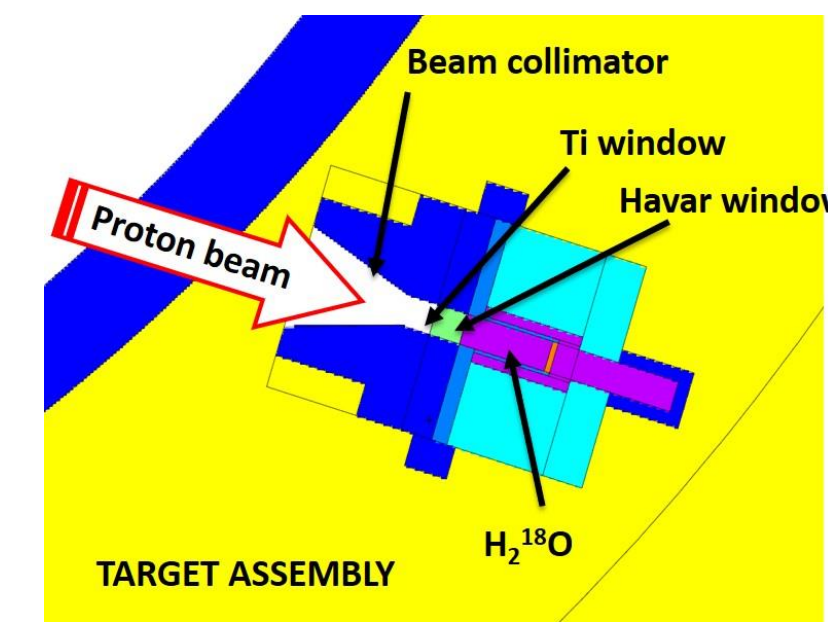


FIGURE 4: MC target model

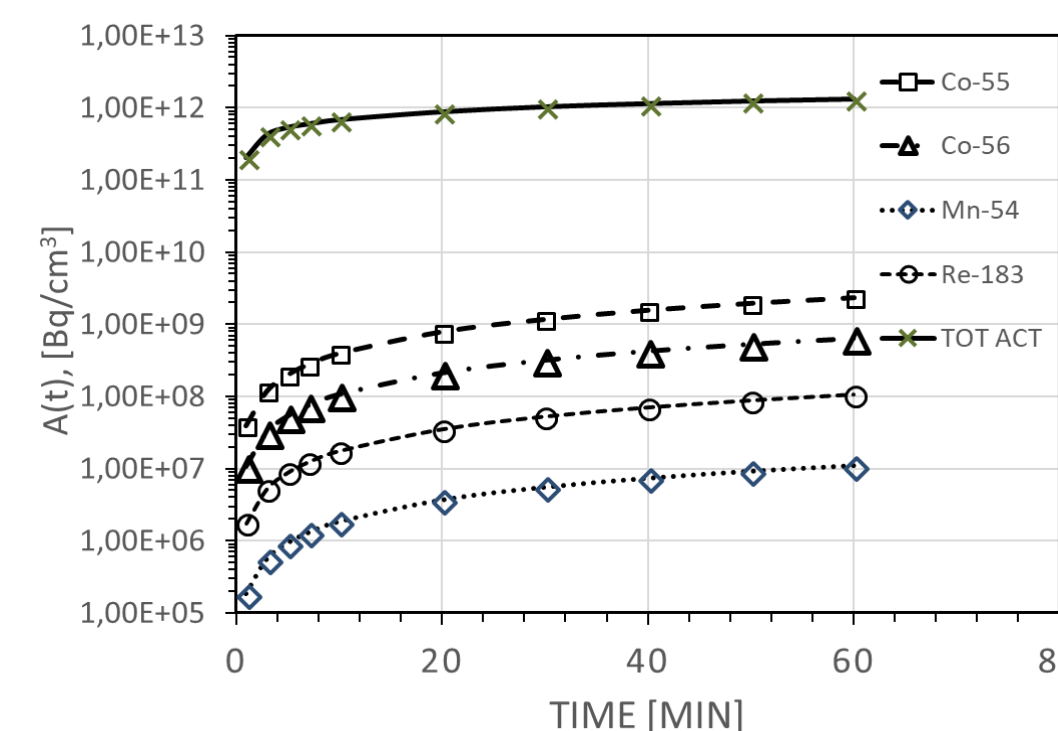


FIGURE 5: Nuclide activities as a function of time

Nuclide	Reaction channel	Calculated Specific Activity [Bq/cc]	Rate [%]	Half-life [s]
^{51}Cr	$^{52}\text{Cr}(p,n+p)^{51}\text{Cr}$	2.6933×10^9	0.19	2.393×10^6
^{55}Co	$^{54}\text{Fe}(p,\gamma)^{55}\text{Co}$	4.0550×10^{11}	28.09	8.160×10^1
^{56}Co	$^{57}\text{Fe}(p,2n)^{56}\text{Co}$	1.6734×10^{11}	11.34	3.294×10^4
^{58}Co	$\text{Ni}(p,x)^{58}\text{Co}$	5.1319×10^{10}	3.55	2.772×10^3
^{52}Mn	$^{52}\text{Cr}(p,n)^{52}\text{Mn}$	6.1231×10^9	0.42	6.314×10^4
^{54}Mn	$^{54}\text{Cr}(p,n)^{54}\text{Mn}$	4.7152×10^9	0.33	4.831×10^4
^{183}Re	$\text{W}(p,x)^{183}\text{Re}$	1.0456×10^8	0.22	6.048×10^6
Total activity		1.4438×10^{12}	-	-

TABLE 1: Calculated specific activities of the dominant radionuclides in the Havar[®] window @ EOB after 60 minutes of irradiation @ 30 μA beam current. The third col-umn (i.e. Rate [%]) represents the percentage over the total activity for the specific radionuclide. Uncertainties for each simulation data on specific activity are less than 5%.

High resolution gamma spectrometry: results

- Gamma spectrometry** (Figure 7) for radionuclidic content evaluation of the irradiated samples has been performed on a low-background HPGe coaxial, vertical dip-stick detector (EG&G ORTEC), which has a relative efficiency of 25–30% and a resolution of 1.95 keV FWHM at 1332 MeV (with a peak to Compton ratio of 55/1). MAESTRO[®] multi-channel Analyzer (MCA) emulation software card, coupled to the detector via electronic modules, all manufactured by EG&G ORTEC. Gamma Vision[®] software has been used for peaks identification and evaluation.
- HPGe detector efficiency calibration curve** (Figure 6) has been obtained using a point-like multigamma source (Am-241, Cd-109, Co-57, Ce-139, Sn-113, Cs-137, Mn-54, Zn-65, Co-60), as reported in Figure 5.

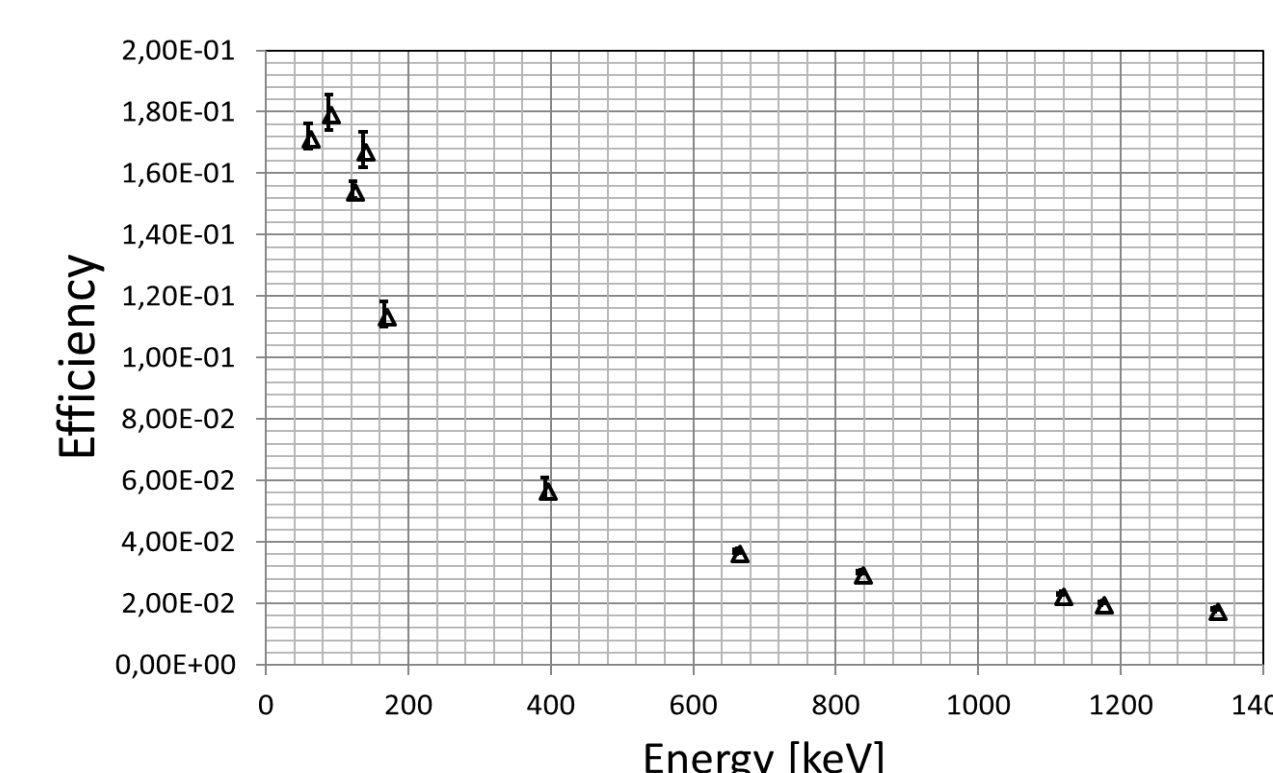


FIGURE 6: Efficiency curve for the HPGe detector.

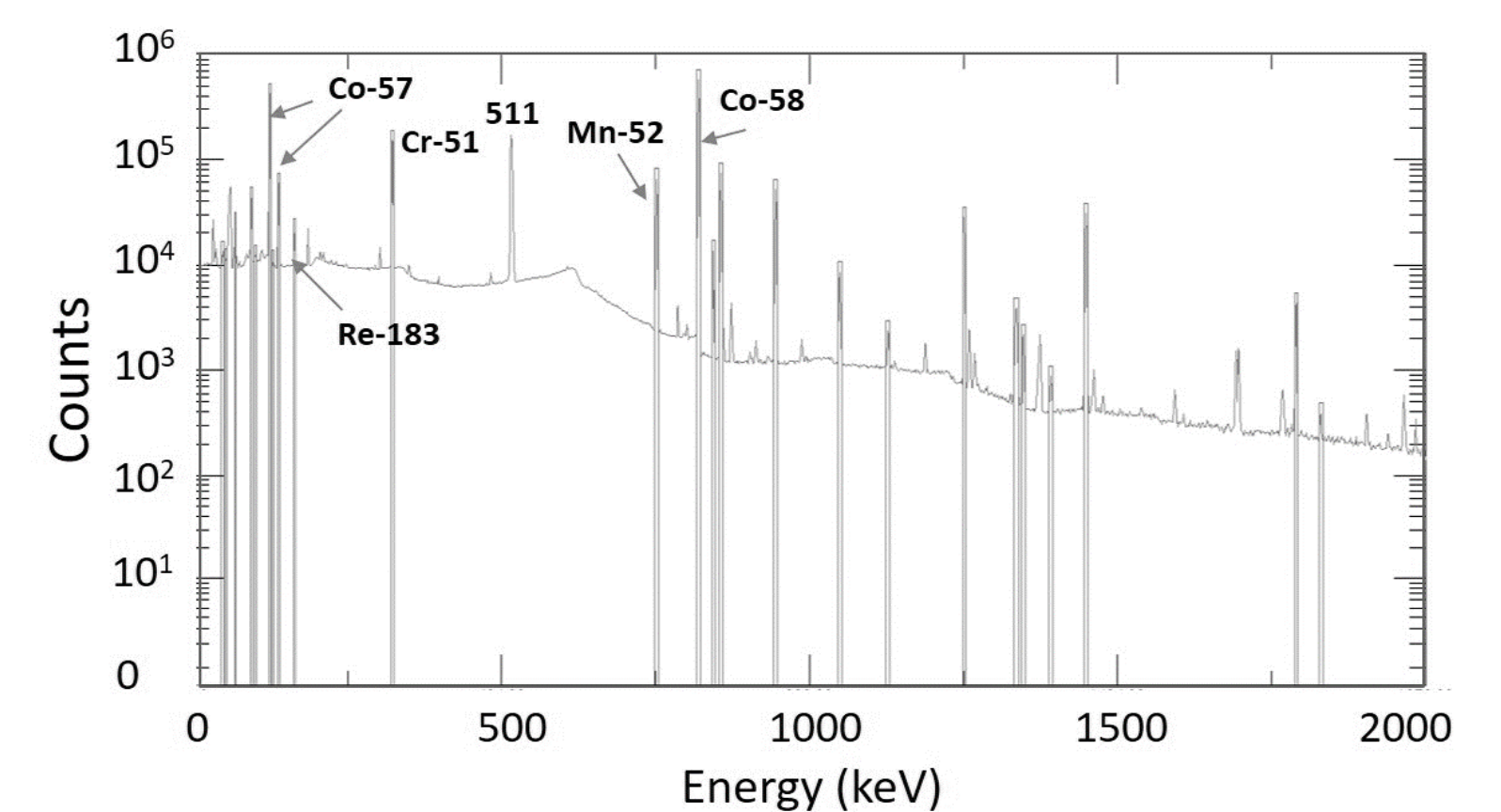


FIGURE 7: Typical gamma spectrum of a sample of irradiated water

- The **comparison simulation and experimental results** (Figure 8) shows that the amount of nuclides produced in Havar[®] window are several orders of magnitude **higher** than the ones measured in the irradiated water, indicating that only a **very small portion of material is released** from the Havar[®] foil to the irradiated enriched-water volume during the bombardment phase following ero-sion/corrosion effects.

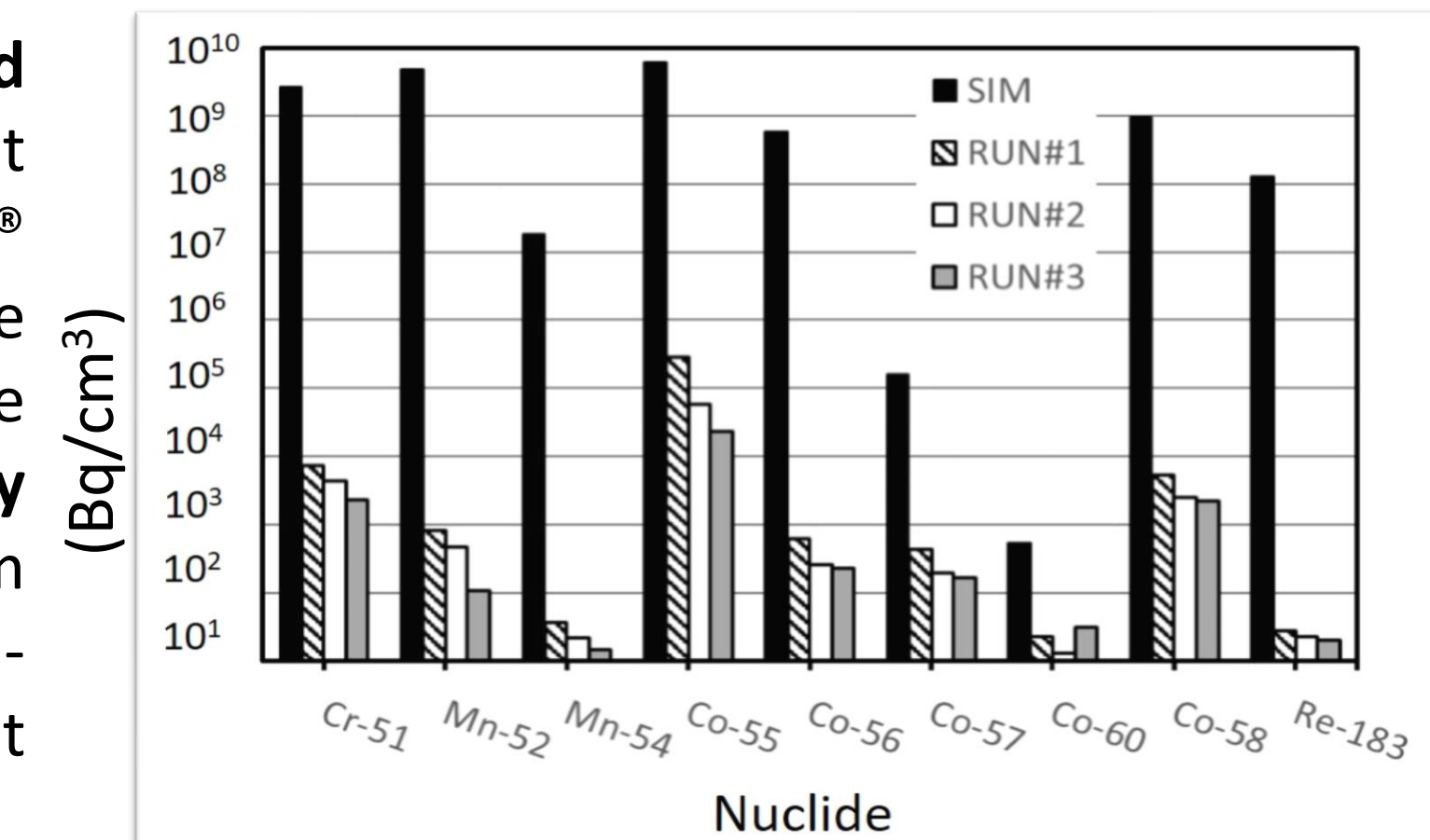


FIGURE 8: experimental specific activity @ EOB for the dominant nuclides compared with simulation results

- This process tends in general to **reduce with time**, irradiation after irradiation. This effect can be explained as the effect of the removal of surface metallic residues at each irradiation mixed with the phenomena of trap-ping the produced nuclides by the surfaces of the target cell.
- Higher initial release of nuclides can be avoided by carefully cleaning all the spare parts involved in target cell maintenance and keeping all the irradiation condition as stable as possible could reduce the probability to introduce further effects on cell target.
- The **study** presented here can be further **extended and applied** to the assessment of radionuclidic purity in case of new target materials directly in contact with the irradiated volume.

ACKNOWLEDGEMENTS

The authors are thankful to Mr. Conan Carette, field engineer from IBA (Ion Beam Application,) for the preparation and cleaning of the target components and for taking care of our machine "LUISONA" during maintenance visits. This research did not receive any specific grant from funding agencies in the public, commercial, or not-for-profit sectors.

References

- Alauddin, M.M., 2012. Positron emission tomography (PET) imaging with ^{18}F -based radiotracers. *American Journal of Nuclear Medicine and Molecular Imaging* 2(1), 55–76.
- Alloni, D., Prata, M., 2017. Characterisation of the secondary neutron field generated by a compact PET cyclotron with MCNP6 and experimental measurements. *Applied Radiation and Isotopes* 128,204–209.
- Bowden, L., Léon Vitró, L., Mitchell, P., O'Donnell, R.G., Seymour, A.M., Duffy, G.J., 2009. Ra-dionuclide impurities in proton-irradiated $[^{18}\text{O}]\text{H}_2\text{O}$ for the production of ^{18}F : activities and distribution in the $[^{18}\text{F}]\text{FDG}$ synthesis process. *Applied Radiation and Isotopes* 67, 248–255.
- Gillies, J.M., Najm, N., Zwert, J., 2006. Analysis of metal radionuclide impurities generated in $[^{18}\text{O}]\text{H}_2\text{O}$ during the cyclotron production of fluorine-18. *Applied Radiation and Isotopes* 64, 431–434.
- IAEA TECDOC 1211, 2001. Charged particle cross-section database for medical radioisotope production: diagnostic radioisotopes and monitor reactions.
- IAEA TECHNICAL REPORTS SERIES No. 468, 2009. Cyclotron produced radionuclides: physical characteristics and production methods.
- Remetti, R., Burgio, N.T., Maciocco, L., Arcese, M., Filanino, A., 2011. Monte Carlo simulation and radiometric characterization of proton irradiated $[^{18}\text{O}]\text{H}_2\text{O}$ for the treatment of the waste streams originated from $[^{18}\text{F}]\text{FDG}$ synthesis process. *Applied Radiation and Isotopes* 69, 1046–1051.
- Sato, T., Niita, K., Matsuda, N. et al., 2013. Particle and Heavy Ion Transport code System, PHITS, version 2.52. *Journal of Nuclear Science and Technology* 50, 913–923.
- Tewson, T.J., Berridge, M.S., Bolomey, L., Gould, K.L., 1988. Routine production of reactive fluo-rine-18-fluoride salts from an oxygen-18 water target. *Nuclear Medicine and Biology* 15,499–504.